Taylor & Francis
Taylor & Francis Group

ORIGINAL RESEARCH

🔓 OPEN ACCESS Check for updates

Acquired DNA damage repairs deficiency-driven immune evolution and involved immune factors of local versus distant metastases in non-small cell lung cancer

Wen-Fang Tang [ID]a*, Xiao-Jun Fanb*, Hua Baob*, Rui Fuc,d*, Yi Lianga*, Min Wub, Chao Zhangc, Jian Suc, Yi-Long Wuc, and Wen-Zhao Zhongc,d

aDepartment of Cardiothoracic Surgery, Zhongshan City People's Hospital, Zhongshan, P. R. China; bGeneseeq Research Institute, Nanjing Geneseeq Technology Inc, Nanjing, P. R. China; cGuangdong Lung Cancer Institute, Guangdong Provincial People's Hospital (Guangdong Academy of Medical Sciences), Southern Medical University, Guangzhou, China; dSchool of Medicine, South China University of Technology, Guangzhou, P. R. China

ABSTRACT

The evolution of immune profile from primary tumors to distant and local metastases in non-small cell lung cancer (NSCLC), as well as the impact of the immune background of primary tumors on metastatic potential, remains unclear. To address this, we performed whole-exome sequencing and immunohisto-chemistry for 73 paired primary and metastatic tumor samples from 41 NSCLC patients, and analyzed the change of immune profile from primary tumors to metastases and involved genetic factors. We found that distant metastases tended to have a decreased CD8+ T cell level along with an increased chromosomal instability (CIN) compared with primary tumors, which was partially ascribed to acquired DNA damage repair (DDR) deficiency. Distant metastases were characterized by immunosuppression (low CD8+ T cell level) and immune evasion (high PD-L1 level) whereas local metastases (pleura) were immune-competent with high CD8+ T cell, low CD4+ T cell and low PD-L1 level. Primary tumors with high levels of CD4+ T cells were associated with distant metastases rather than local metastases. Analysis of TCGA data and a single-cell RNA-sequencing dataset revealed a decreasing trend of major immune cells, such as CD8+ T cells, and an increasing trend of CD4 T helper cells (Th2 and Th1) in primary tumors with metastases from local to distant sites. Our study indicates that there are differences in the immune evolution between distant and local metastases, and that acquired DDR deficiency contributes to the immunosuppression in distant metastases of NSCLC. Moreover, the immune background of primary tumors may affect their metastatic potential.

Introduction

Although the treatment of non-small cell lung cancer (NSCLC) has been revolutionized by the use of tyrosine kinase inhibitor (TKI) and immune treatments[1,2], metastatic NSCLC remains largely incurable, and causes the majority of deaths[3]. A better understanding of drivers of metastasis is therefore needed to improve survival outcomes.

Recent studies have begun to shed some light on factors driving the metastatic potential in NSCLC. Metastatic spread requires a permissive immune microenvironment, facilitated by recruitment of immunosuppressive immune cells, such as CD4+ regulatory T cells, and suppression or exhaustion of tumor eliminating immune cells such as CD8+ cytotoxic T cells[4]. In NSCLC, a lot of studies have shown immunosuppression at sites of metastasis. One study found low CD8+ T cell density and low CD8+ to CD4+ T cell ratio in metastasis to various sites[5], confirmed in another recent study[6]. One study focusing on brain metastasis also found sparse T cell density in the metastasis of NSCLC patients[7]. While NSCLC metastasis

has proven to be immunosuppressive, whether the immune status of the primary tumor affects the metastatic potential of NSCLC remains an open question. Early murine models have shown recruitment of immunosuppressive cells to site of primary tumor encourages tumor cell dissemination and increase metastatic potential[4], whether a similar phenomenon occurs in NSCLC is of great interest. Greater metastatic potential is needed for metastatic cells to survive in circulation and colonize distant sites, as oppose to nearby locale[8]. Whether the primary tumor immune status influences metastatic potential to disseminate to distant versus local sites is unknown.

Theoretically, there are two ways by which metastases can attain the immunosuppressive nature: metastatic cells could have derived this immunosuppressive capability from the primary tumor, where the primary tumor cells could already have the ability to create an immunosuppressive environment, and metastatic cells merely inherit this ability. Or, immunosuppressive capability could have been acquired during the metastatic dissemination process. For the latter scenario, a high level of

genomic instability could be responsible, as shown in a recent study where metastases have significantly higher genomic instability compared to primary[6]. Particularly, recent studies have discovered that high chromosomal instability (CIN) is associated with low level of CD8+ T cells[9], and CIN can drive metastasis through deregulated cGAS – STING (cyclic GMP-AMP synthase – stimulator of interferon genes) pathway by interfering the innate immune response in tumors[10,11]. Considering the key role of DNA damage repair (DDR) mechanism in the maintenance of CIN, it is of great interest to understand how aberrant DDR mechanism promote NSCLC metastasis by affecting CIN and further impacting the immunophenotype of metastasis[12,13].

In this study, we recruited a cohort of 41 NSCLC patients and sequenced 73 samples. By using whole-exome sequencing and immunohistochemistry, we aim to examine the variations in immune status and key genetic characteristics among the primary tumors, local, and distant metastases of NSCLC, to identify the factors that contribute to these differences, specifically those that trigger immunosuppression in metastases, with a focus on DDR and associated CIN, and to investigate the impact of the immune profile of primary tumors on their metastatic destinations (local or distant), so as to understand how the immune profiles evolve from primary tumors to both local and distant metastases in NSCLC.

Materials and methods

Patient cohort and sample collection

Primary tumor (PT) and metastatic tumor (MT) samples from a total of 41 patients with metastatic NSCLC were collected for this study. Patients were treated at the Guangdong Provincial People's Hospital from 2010 to 2019. PT samples were treatment naive and MT samples did not receive any systemic treatment. Follow-up ended at August 11, 2021. The median follow-up time was 28 months (IQR: 18.6–39.0 months). The study was approved by the ethics committee of the institute, and all included patients signed informed consent forms. All formalin-fixed, paraffin-embedded specimens were subjected to whole-exome sequencing (WES) and immunohistochemistry of CD4, CD8 and PD-L1. After filtering by tumor purity (≥0.2), total QScore of DNA damage (≥35) evaluated by Picard tool (http://broadinstitute.github.io/picard/) and contamination (<0.05), there were 73 samples were included in the study.

External datasets

We used the TCGA data to validate our results and further explore which exact immune cell subsets are involved in lung cancer metastasis. The enrichment score data of 64 immune and stromal cell types in the TCGA lung adenocarcinoma primary tumors were pre-calculated by xCell[14] and downloaded from the xCell website (https://xcell.ucsf.edu/). A total of 402 patients with clear pathological TNM stage information were included in the analysis. According to patient's pN and pM information, we divided the patients into 4 groups: N0-M0 group (no metastasis, pN=N0 and pM=M0, $n = 216$), N1 group (pM=M0, pN=N1, $n = 90$), N2-N3 group (pM=M0, pN=N2 or

N3, $n = 71$), and M group (intrathoracic or distant metastasis, pM=M1, M1a, M1b or M1c, $n = 25$). Such grouping basically reflects the process of metastasis from local to distance or from near to far sites.

We also used a single-cell RNA-sequencing dataset to investigate which T cell subset is associated with metastatic potential of lung cancer cells at single-cell level[15]. The original data include 12,346 T cells and 12,415 genes from 14 treatment-naïve non-small-cell lung cancer patients. The processed raw count dataset was downloaded from GEO (https://www.ncbi.nlm.nih.gov/geo/) with accession code of "GSE99254". The raw counts were then log-normalized by Seurat package[16]. Among 12,346 T cells (including T cells from peripheral blood, adjacent normal tissue and tumor tissue), we selected 5,616 tumor tissue infiltration T cells for subsequent analysis. The 5,616 T cells included 3,547 cells from stage I patients, 1,567 cells from stage III patients and 502 cells from stage IV patients. We annotated the cells using a reference based method. Specifically, ProjecTILs package[17] was used to project new scRNA-seq data into a reference without altering its structure. The reference atlas contains 9 tumor-infiltrating T cell subsets. After annotation, we calculated the proportions of various T cell subsets in stage I, III and IV cells.

DNA extraction, library construction, and whole exome sequencing

DNA from tissue samples and blood samples were extracted using a DNeasy Blood & Tissue Kit (Qiagen). All DNA samples were quantified by Qubit 3.0 using the dsDNA HS Assay Kit (Life Technologies). Sequencing libraries were prepared using the KAPA Hyper Prep Kit (KAPA Biosystems). Target enrichment was performed using the xGen Exome Research Panel and Hybridization and Wash Reagents Kit (Integrated DNA Technology, USA). Libraries were subjected to PCR amplification with KAPA HiFi HotStart ReadyMix (KAPA Biosystems). Sequencing was performed on Illumina HiSeq4000 platform using PE150 sequencing chemistry (Illumina, USA) to a mean coverage depth of 150× for tissue samples, and 60× for matched normal control blood samples.

Somatic mutation detection

FASTQ file quality control was performed using Trimmomatic[18], where N bases and low quality (score <20) bases were removed. Pair-end reads were aligned to the human reference genome (hg19) using Burrows-Wheeler Aligner (BWA) with default parameters[19], followed by PCR deduplication with Picard V2.9.4 (Broad Institute, MA, USA). Local realignment around indels and base quality score recalibration was performed with the Genome Analysis Toolkit (GATK 3.4.0)[20]. Somatic single-nucleotide variants (SNVs) were identified using MuTect2[21]. Final list of mutations was annotated using vcf2maf (https://github.com/mskcc/vcf2maf). The resulting mutation list was filtered through an internally collected list of recurrent sequencing errors on the same sequencing platform, summarized from the sequencing results of 500 normal samples. Mutations occurring within repeat masked regions were also removed. Somatic mutation calls were

further filtered using the following criteria: (i) minimum 4 reads supporting the variant; (ii) ≥5% variant allele frequency (VAF); (iii) not present in public databases (Exome Variant Server, 1,000 genomes project and Exome Aggregation Consortium) at population frequency >1%.

Copy number alteration analysis

FACETS[22] was used to estimate tumor purity, segment-level somatic copy number alterations (SCNAs) and ploidy. Gene-level SCNAs were determined and assigned a 5-grade scale according to the purity-adjusted total copy number and ploidy of the segment where the gene is located. The 5-grade scale was shown in Supplementary Table S4. We used CNApp online tool[23] to calculate focal SCNA score (FCS) and broad SCNA score (BCS) of each sample. We defined focal SCNAs were SCNAs that covered less than 60% of a chromosomal arm; otherwise, broad SCNAs. The weight of each broad or focal SCNA event was also assigned on the basis of the above 5-grade scale.

Mutational signature analysis

De novo single base substitution (SBS-96) signature extraction and decomposition of extracted signatures to known COSMIC signatures (http://cancer.sanger.ac.uk/cosmic/signatures) were performed with SigProfiler tools (https://github.com/AlexandrovLab/SigProfilerExtractor) based on nonnegative matrix factorization (NMF) algorithm[24]. We extracted mutation signatures from mutations in the primary tumors representing baseline mutation processes, and also extracted mutation signatures from non-lymph node metastasis-specific mutations (mutations only existed in the pleural, brain, bone, and adrenal gland metastases) and lymph node metastasis-specific mutations (mutations only existed in the lymph node metastases), which represent acquired mutation processes during metastasis.

Cancer gene and DNA damage repair (DDR) gene annotation

Cancer genes were annotated with the OncoKB Database (https://www.oncokb.org/). Only genes whose function is definite, that is, labeled as "Oncogene" or "Tumor Suppressor Gene", were included. For DDR genes, genes belonging to the 7 KEGG pathways involved in DNA damage repair including "P53_SIGNALING_PATHWAY", "FANCONI_ANEMIA_PATHWAY", "HOMOLOGOUS_RECOMBINATION", "MISMATCH_REPAIR", "BASE_EXCISION_REPAIR", "NON_HOMOLOGOUS_END_JOINING" and "NUCLEOTIDE_EXCISION_REPAIR", at the same time, belonging to cancer genes, were included in the analysis (Supplementary Table S3).

dNdscv analysis

We assessed whether mutations in DDR pathway underwent positive selection during distant metastasis via dNdScv tool[25]. dNdScv estimates the ratio of non-synonymous to synonymous mutations based on a Poisson regression algorithm. To compare the selection of DDR pathway mutations in primary tumors and non-lymph node metastases, we only included 22 paired primary and non-lymph node metastatic samples to ensure the sample size of primary and metastatic group was same (2 paired samples lacked DDR cancer gene mutations in both primary and metastatic samples, and were not included). For pathway-level analysis, input was mutations of genes belonging to a pathway, and the global dN/dS estimation represents the selection of the pathway as a whole in the cohort.

Cancer cell fraction (CCF) estimation

Pyclone (v0.13.0)[26] was used to estimate CCF of each mutation. Only non-synonymous mutations were included. Tumor purity, minor copy number, major copy number estimated by FACETS, as well as reference read count and alternate read count were input to Pyclone to estimate mutation CCF and its standard deviation. Clonal mutations were mutations whose upper bound of 95% confidence interval of CCF ≥1.

Immunohistochemistry (IHC)

Formalin-fixed, paraffin-embedded tissue blocks were sectioned at 4 μm and mounted on glass slides, and then immune-stained for PD-L1 (22C3 clone, DAKO, Carpinteria, CA, USA), CD8 (C8/144B clone, Gene Tech Co. Ltd., Shanghai, China) and CD4 (EP204 clone, Gene Tech Co. Ltd., Shanghai, China). PD-L1 expression level was measured with tumor proportion score (TPS), which is the proportion of total viable tumor cells showing partial or complete membrane PD-L1 staining. TPS positive if TPS ≥1%, otherwise negative. The levels of CD8+ or CD4+ T cells were measured as the proportion of CD8+ T cells or CD4+ T cells among nucleated cells in the stromal compartment of each slide. CD4 or CD8 positive was defined as positive if CD4+ or CD8+ T cell proportion ≥5%, otherwise negative.

Statistical analysis

Non-parametric Wilcoxon's rank-sum test was used to assess difference of numerical features between two groups. For comparison among multiple groups, Kruskal–Wallis method was used to test overall statistical significance and pairwise Wilcoxon's test was used for post hoc analyses. Jonckheere's trend test was used to test increasing or decreasing trend of numerical features in multiple ordered groups (one-sided test). Comparisons of proportion between groups were done using the Fisher's exact test. For survival analyses, Kaplan–Meier curves were compared using the log-rank test. A two-sided P value of less than 0.05 was considered significant for all tests unless indicated otherwise. For multiple tests, P values were adjusted using the Benjamini–Hochberg method. All statistical analyses were performed with R packages (v.3.5.3).

Results

Clinicopathological characteristics and genomic landscape

The present study included 41 patients with metastatic NSCLC. The majority had adenocarcinoma (36, 87.8%). The median age was 56 years old (range 34–81). Among 41 patients, 31 (75.6%) were synchronous metastases, and 10 (24.4%) were metachronous metastases. For synchronous metastasis, progression-free survival (PFS) was the interval between the initial diagnosis and the first progression. For metachronous metastasis, PFS was the interval between the surgery of primary tumor and the detection of the first metastasis. Detailed patient information was shown in Supplementary Table S1.

A total of 73 samples with both sequencing data and IHC data were included in this study. The 73 samples contained 29 primary tumors, 9 lymph node metastases, 9 pleura metastases (PL), 9 brain metastases (BR), 10 bone metastases (BN), and 7 adrenal gland metastases (AD). We defined PL metastases as local metastases, and BR, BN, and AD metastases as distant metastases. There were 31 primary-metastasis pairs including 7 primary-lymph node pairs and 24 primary-non-lymph node pairs. Cohort information was shown in Supplementary Fig.S1. Considering that tumor purity may affect mutation and CNV calling, we compared tumor purity in primary tumors and various metastatic organs, no significant difference in tumor purity was observed (Supplementary Fig.S2). Detailed sample information was shown in Supplementary Table S2.

As expected, *TP53* and *EGFR* were the most frequently mutated genes, and the majority were clonal mutations, followed by *KMT2A*, *KMT2D* and *KMT2C* (Supplementary Fig. S3A). We found multiple genes involved in DNA damage repair were more likely to be mutated in PL/distant metastases compared with primary tumors, including *ATR* (0% vs. 14.3%, $P = 0.06$), *FANCA* (3.4% vs. 14.3%, $P = 0.21$), *BRCA1* (3.4% vs. 11.4%, $P = 0.37$), *BRCA2* (6.9% vs. 14.3%, $P = 0.44$) or any one of the above 4 genes (13.8% vs. 42.9%, $P = 0.01$) (Supplementary Fig.S3B), suggesting DNA damage repair deficiency may play a role in NSCLC metastasis.

Aberrant DNA damage repair pathway was associated with metastasis

In view of the above finding, we first used dNdScv method to investigate whether mutations in DDR pathway underwent positive selection in metastases. We combined metastases of PL, BR, BN and AD to form the non-lymph node metastasis group. We found dN/dS ratios of all types of mutations in DDR pathway genes increased in the non-lymph node metastases compared with primary tumors although not significant due to sample size (overlap of 95% confidence interval of dN/dS ratio). In addition, the dN/dS ratios of all loss-of-function mutations (truncation, splicing, and nonsense) and overall mutations were significantly greater than 1 in the metastases and not significant in primary tumors given same sample size (Figure 1A). Consistent with this finding, we found SBS3, a mutation signature associated with homologous recombination repair (HRR) deficiency, was uniquely seen in non-lymph node metastasis-specific mutations (dark green) but absent from primary tumor mutations (Figure 1B), suggesting DDR deficiency may be an important factor driving NSCLC metastasis.

Further analysis found that CCF of mutations in the DDR pathway increased more in the metastases with SBS3 signature than those without SBS3 signature (Figure 1C). For specific DDR pathways, the difference of CCF increase was significant in the Fanconi anemia pathway ($P = 0.007$) and showed trend toward significance in HRR pathway ($P = 0.18$) (Figure 1D). *BRCA1*, *BRCA2*, *FANCA* and *ATR* gene, which showed a trend of being enriched in metastases, are members of the Fanconi anemia pathway (Supplementary Table S3). As expected, SBS3 signature was closely related to genomic instability, where polyploid metastases had significantly greater proportion of SBS3 signature (Figure 1E). SBS3-positive metastases also had significantly higher BCS (broad somatic copy number alteration score) and higher tumor mutational burden (TMB) compared to SBS3-negative metastases (Figure 1F,G). Additionally, the SBS3 positive rates tended to be higher in the distant metastases (BR/BN/AD) than PL metastases although not significant ($P = 0.1$) (Figure 1H).

Immunosuppression was found in distant metastases along with increased chromosomal instability

We then compared CD8, CD4 and TPS in primary tumors, lymph node metastases, local (pleural) and distant metastases. Although due to limited sample size, the overall difference in CD8+ T cell level among the 4 groups did not achieve statistical significant ($P = 0.06$, Figure 2A), it could be observed that distant metastases tended to have the lowest CD8+ T cell level (Figure 2A). Different from CD8, CD4+ T cell level appeared to be the lowest in the local metastases, particularly when in comparison with distant metastases ($P = 0.011$) (Figure 2B). Similarly, pleural metastases also tended to have a lower TPS than distant metastases ($P = 0.038$) (Figure 2C), despite that the overall and "BH" adjusted p-values were greater than 0.05 because of a small sample size in individual groups. In summary, distant metastases rather than local metastases were characterized by immunosuppression (low CD8+ T cell) and immune evasion (high TPS level)[27;] while local metastases were characterized by low level of both CD4+ T cell and TPS. We also analyzed the correlation between the levels of CD8, CD4 and TPS. When considering all samples, there was no significant correlation observed between the three markers (Supplementary Fig.S4A-S4C). However, in distant metastases, there appeared to be a weak positive correlation between CD8 and TPS (Supplementary Fig.S4D-S4F). For instance, CD8-positive distant metastases tended to have a higher TPS level ($P = 0.1$, Supplementary Fig.S4E) or a higher TPS-positive rate ($P = 0.05$, Supplementary Fig.S4F) than CD8-negative distant metastases.

CIN has been shown to induce metastasis[10]. Reports also show CIN is associated with the decrease of CD8+ T cell level[9]. Our results showed CIN increased in the distant metastases instead of local metastases. Polyploidy rate in the distant metastases was significantly higher compared with primary tumors ($P = 0.03$, Figure 2D). FCS and BCS, particularly BCS, were also higher in the distant metastases ($P = 0.093$ and $P =$
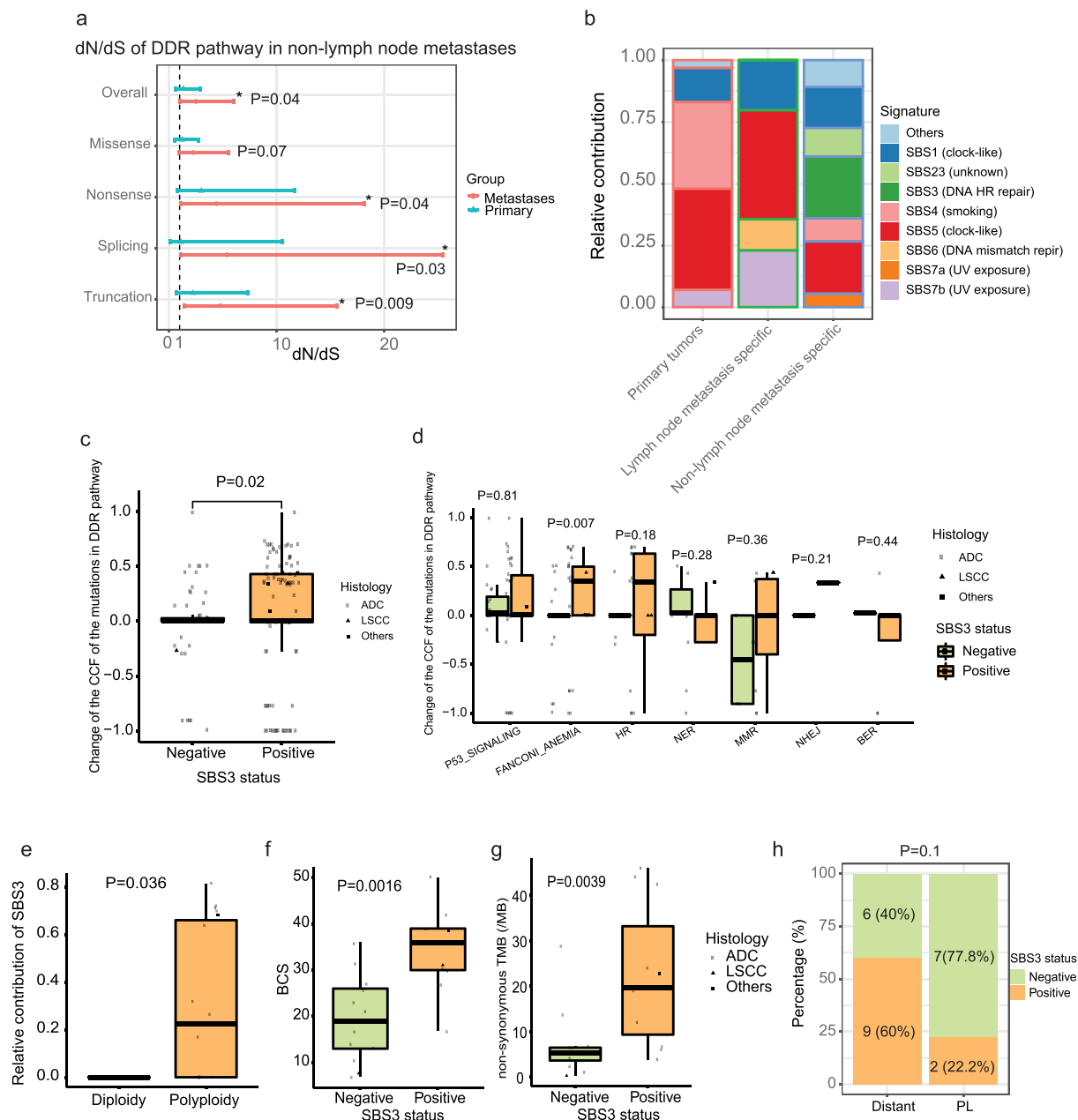
Figure 1. Association between DNA repair pathway, mutation signature SBS3 and chromosomal instability in primary and metastatic NSCLC tumors. (A) dN/dS analysis of the mutations of cancer-related genes in the DDR pathway in the primary tumors and non-lymph node metastases by dN/dScv method. To ensure same sample size, only paired samples were included (n = 22 pairs, 2 paired samples lacked DDR cancer gene mutations in both primary and metastatic samples, and were not included). Bar represents 95% confidence interval of dN/dS and * represents dN/dS is significantly greater than 1 (P ≤ 0.05). (B) mutations were classified into three groups: primary (29 samples), lymph node metastasis specific (7 samples) and non-lymph node metastasis specific (24 samples, including PL, BR, BN and AD), for metastases, only paired samples were included. COSMIC mutation signatures were extracted from each group by the SigProfiler tools. The relative contributions of the signatures in the three groups were plotted. (C) changes of the CCF of the mutations of cancer-related DDR genes in the paired non-lymph node metastases stratified by SBS3 status (negative = 11, positive = 11, two samples without cancer-related DDR gene mutations were not included), each dot represents a mutation. (D) changes of the CCF of the mutations in different KEGG DDR associated pathways in the paired non-lymph node metastases stratified by SBS3 status. (E) the relative contribution of SBS3 signature in the paired non-lymph node metastases (n = 24) stratified by ploidy status (diploidy = 5; polyploidy = 19). (F) BCS in the non-lymph node metastases (n = 24) stratified by SBS3 status (negative = 13; positive = 11). (G) TMB in the non-lymph node metastases (n = 24) stratified by SBS3 status (negative = 13; positive = 11). (H) distribution of SBS3 status in the distant metastases (BR, BN and AD) and PL metastases. AD: adrenal gland; ADC, adenocarcinoma; BCS: broad copy number alteration score; BER: base excision repair; BN: bone; BR: brain; CCF: cancer cell fraction; DDR: DNA damage repair; HR: homologous recombination; LSCC, lung squamous cells carcinoma; MMR: mismatch repair; NER: nucleotide excision repair; NHEJ: non-homologous end joining; PL: pleural; TMB: tumor mutation burden.

0.0037 for FCS and BCS, Figure 2E,F). On the contrary, CIN in the lymph node metastases and PL metastases did not show significant difference compared to the primary tumors (Figure 2D–F). Paired primary-metastasis comparison further supported the increase of CIN in the distant metastases (Figure 2G,H).

## Association between DDR deficiency, genomic instability and immunosuppression

We found CD8+ T cell level was lower in polyploid samples than diploid samples (Figure 3A). In addition, on the basis of polyploidy, FCS seemed to be associated with CD8+ T cell level
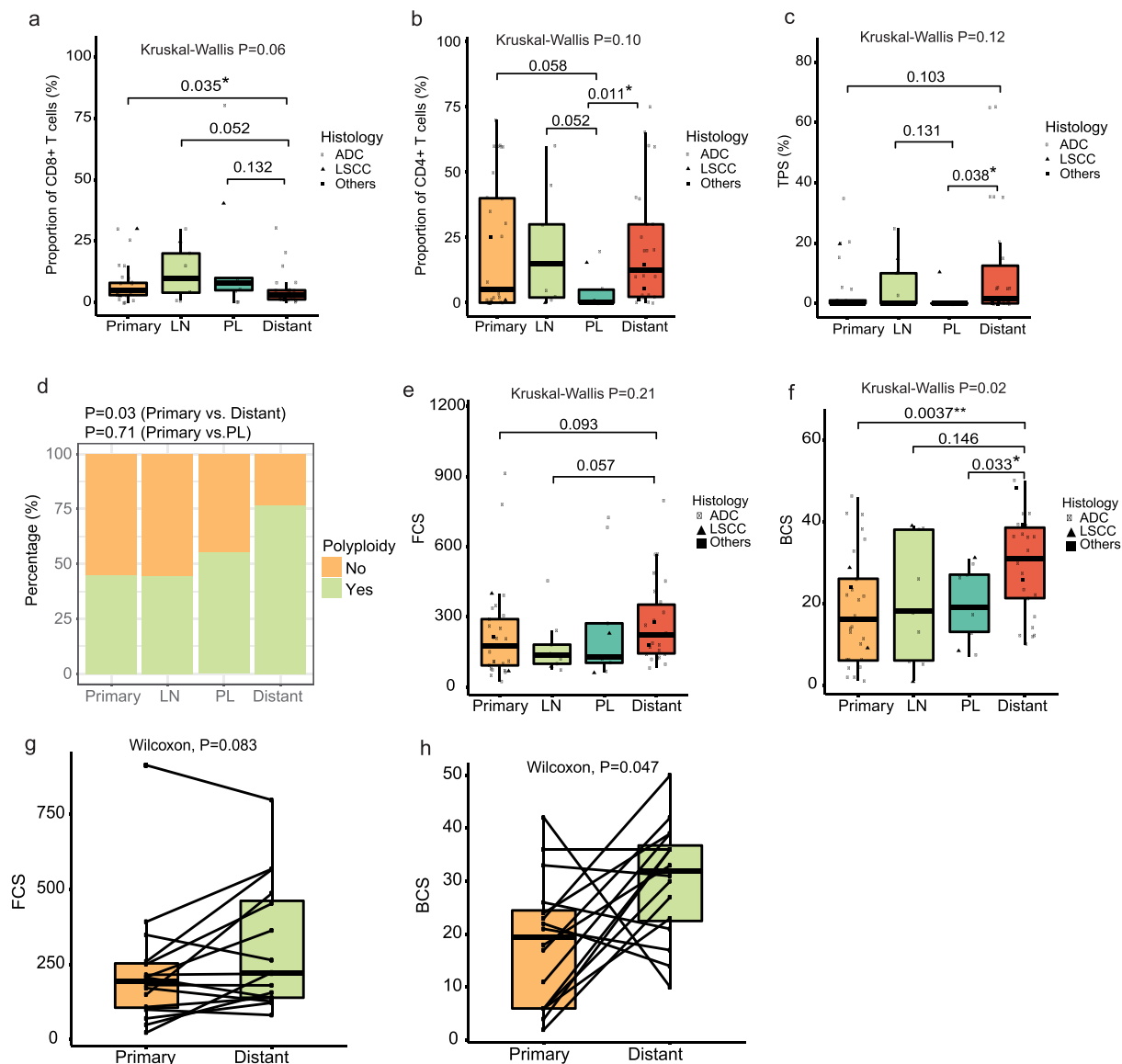
Figure 2. Immune profile and chromosomal instability in primary tumors and metastases. (A-C) comparison of the levels of CD8+ T cells, CD4+ T cells and TPS among primary tumors ($n = 29$), lymph node metastases (LN, $n = 9$), PL metastases ($n = 9$) and distant metastases including BR (brain, $n = 9$), BN (bone, $n = 10$) and AD (adrenal gland, $n = 7$). The numbers on the top of the bars represent p-values of pairwise Wilcoxon tests. * represents p-value ≤0.05. For A-C, all "Benjamini-Hochberg" adjusted p-values >0.05. (D) distribution of polyploidy in primary, lymph node metastasis, PL and distant metastases. (E-F) comparison of FCS and BCS among primary tumors, lymph node metastases (LN), PL metastases and distant metastases. The numbers on the top of the bars represent p-values of pairwise Wilcoxon tests. * represents p-value ≤0.05; ** represents both p-value and "Benjamini-Hochberg" adjusted p-value ≤0.05. (G-H) paired comparison of FCS and BCS between the primary tumors and distant metastases ($n = 15$ pairs). BCS: broad copy number alteration score; FCS: focal copy number alteration score; TPS: tumor proportion score.

more significantly than BCS (Figure 3B,C). Dynamic analysis showed a negative correlation between CD8 change and FCS change in the 31 paired primary-metastasis samples (Spearman's ρ=−0.47, $P = 0.008$) (Figure 3D). Despite lacking statistical significance, it appeared that the relative contribution of SBS3 signature in the PL/distant metastases showed a contrasting trend in relation to CD8 and CD4 status. Specifically, CD8-negative metastases exhibited a tendency toward a higher SBS3 contribution compared to CD8-positive metastases (Figure 3E), while CD4-negative metastases displayed a tendency toward a lower SBS3 contribution compared to CD4-positive metastases (Figure 3F). As a result, SBS3 contribution showed a positive correlation with CD4-to-CD8 ratio (Figure 3G) and a negative correlation with the change of CD8 + T cell level (Figure 3H). By tracking the CD8 status change

from the primary tumors to their paired PL and distant metastases stratified by SBS3 status (Figure 3I), it was found that among 13 SBS3-negative metastases (cyan bands in the plot), only 3 (23%, 3/13) changed from CD8 positive to negative. Among 11 SBS3-positive metastases (pink bands in the plot), 5 (45.5%, 5/11) changed from CD8 positive to negative. We also noticed that although 4 SBS3-positive metastases still maintained CD8 positivity, their median SBS3 contribution was 0.27, which was lower than 0.68 of another 5 SBS3-positive metastases where CD8 status changed from positive to negative. In addition, although high TMB is also a sign of genomic instability, it was not significantly correlated with CD8+ T cell level. In multivariable linear regression analysis incorporating ploidy status, FCS, TMB, tumor location and histology, only polyploidy maintained its significance with CD8+ T cell level
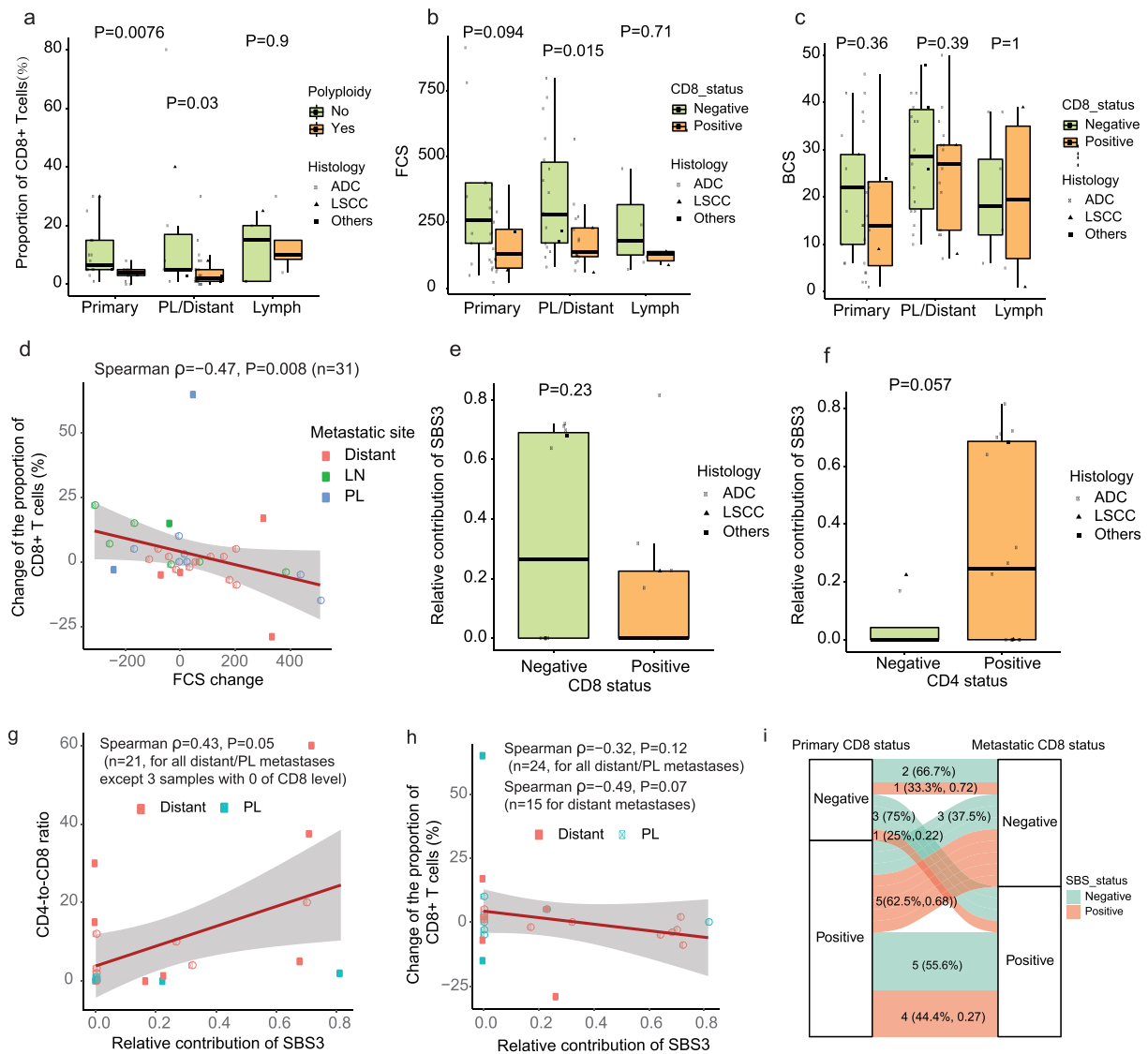
Figure 3. Immunosuppression in the distant metastases along with increased chromosomal instability induced by acquired DDR deficiency. (A) association of CD8+ T cell with ploidy status in primary tumors (n = 29), PL and distant metastases (n = 35), and lymph node metastases (n = 9). (B) FCS levels in primary tumors (n = 29), PL and distant metastases (n = 35), and lymph node metastases (n = 9) stratified by CD8 status. (C) BCS levels in primary tumors (n = 29), PL and distant metastases (n = 35), and lymph node metastases (n = 9) stratified by CD8 status. (D) correlation between CD8 change and FCS change in all paired primary-metastatic tumors (n = 31 pairs). (E) relative contributions of SBS3 signature in the 24 paired non-lymph node metastases (including PL and distant metastases) stratified by CD8 status. (F) relative contributions of SBS3 signature in the 24 paired non-lymph node metastases stratified by CD4 status. (G) correlation between SBS contribution and CD4-to-CD8 ratio in the 21 paired non-lymph node metastases (3 samples with 0 of CD8 level were not included). (H) correlation between CD8+ T cell level change and SBS3 contribution in the 24 paired non-lymph node metastases. (I) change of CD8 status from primary to metastases (24 pairs including PL and distant metastases) stratified by SBS3 status. There are 4 types of CD8 status change (negative-to-negative, negative-to-positive, positive-to-negative and positive-to-positive), for each type of change, there are SBS3 positive cases and negative cases. For example, there are 3 cases of negative-to-negative change (the top two bands), and 2 cases are SBS3 negative and 1 case is SBS3 positive, and the number (0.72) in the positive SBS3 case group indicates the relative contribution of SBS3 signature in the SBS3 positive group. If a group contains multiple SBS3 positive cases, the number represents the median value of SBS3 relative contribution.

(P = 0.03); while TMB was not significant (P = 0.68), suggesting the effect of DDR deficiency on immune status is mainly mediated by CIN involving aneuploidy.

A case is provided in Figure 4. In this patient, the CD8+ T cell was 30% in primary tumor and decreased to 1% in bone metastasis (Figure 4A). Mutation signature analysis showed that bone metastasis-specific mutations contained SBS3 signature (Figure 4B). CIN increased remarkably from primary tumor to bone metastasis as revealed by FACETS (Figure 4C), and clonal evolution analysis identified a clone containing ATR and CCNE1 mutations that underwent expansion in bone metastasis (Figure 4D). Both ATR and CCNE1 are

the members of DDR and participate in the maintenance of chromosomal stability (Suplementary Table S3).

Immune background of primary tumor determines local versus distant metastasis

We have shown distant metastases tended to have lower CD8+ T cell, higher CD4+ T cell and higher TPS levels compared to local metastases (Figure 2A–C). There are two possible mechanisms to explain such a difference. One is dynamic change from primary tumors to metastases. For example, CD8+ T cell may decrease from primary tumor to distant
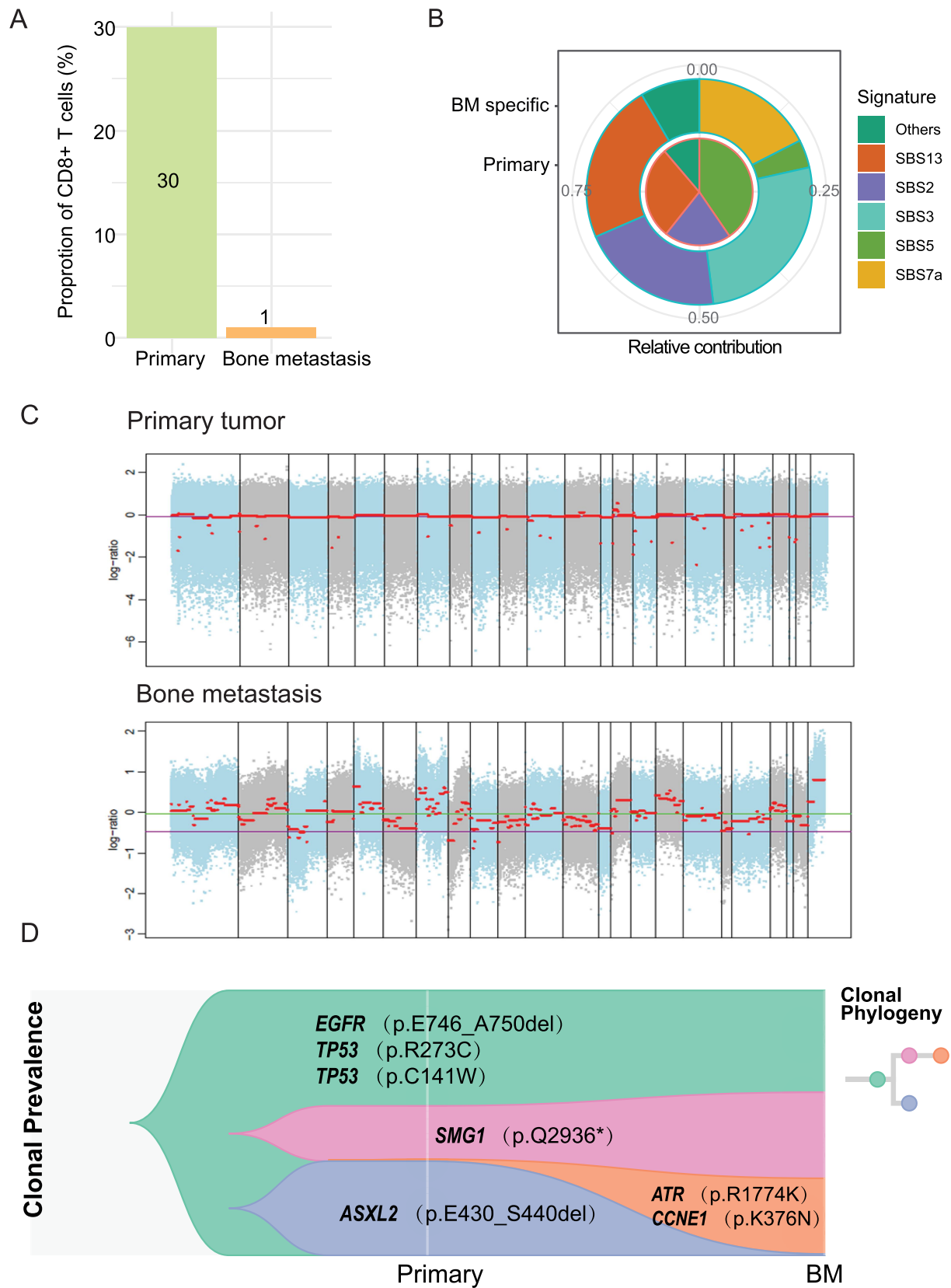
Figure 4. A case of immunosuppression in bone metastasis (BM) driven by acquired DNA repair deficiency. (A) CD8+ T cell level decreased from 30% in primary tumor to 1% in bone metastasis in a patient. (B) mutation signatures extracted from primary mutations (inner) and metastasis specific mutations (outer) in this patient. (C) copy number variation profile (log R ratio estimated by FACETS tool) in primary tumor and bone metastasis in this patient. (D) fish plot show clonal evolution from primary tumor to bone metastasis in this patient.

metastasis, whereas it remains unchanged in local metastases (PL). An alternative mechanism is that the immune profile of primary tumor determines or affects metastatic destinations. For example, if primary tumors with a high CD8+ T cell level are prevented from spreading to distant organs, while permitted to spread to local PL. This process can also result in the higher CD8+ T cell level in PL, even though CD8 did not dynamically change during metastasis. To explore these two possible mechanisms, we tracked the change of CD8, CD4 and TPS status from primary tumors to PL or distant metastases separately (Figure 5A–C). For CD8, the overall concordance was 50% (12/24), and 50% had status conversion in which 66.6% (8/12) underwent positive-to-negative conversion. Among the 8 positive-to-negative cases, 6 took place in distant metastases and 2 took place in PL. The lower SBS3-positive rate (i.e. DDR deficiency rate) in PL (Figure 1H) may explain the fewer positive-to-negative conversions in PL. Secondly, we analyzed whether CD8 status of primary tumors affects metastatic site. Among CD8-negative primary tumors, 14.3% metastasized to PL and 85.7% to distant metastases; and among CD8-positive primary tumors, 47% metastasized to PL and 53% to distant metastases [$P = 0.19$, Fisher exact test was used to compare the difference of metastatic destinations (PL vs. distant) between CD8-negative primary tumors and CD8-positive primary tumors] (Figure 5A). Although not significant, there is a trend toward CD8-negative primary tumors being inclined to spread to distant organs. For CD4, majority (87.5%) were concordant, only 12.5% underwent conversion during metastasis, suggesting the second mechanism may play a major role (Figure 5B). In contrary to CD8, it was observed that CD4-positive primary tumors tended to metastasize to distant organs (12/15, 80%) whereas in CD4-negative primary tumors, 33.3% (3/9) underwent distant metastasis ($P = 0.036$). Similar phenomenon was seen in TPS although not significant ($P = 0.19$) where TPS-positive primary tumors tended to metastasize to distant organs (Figure 5C).

We then divided 29 primary tumors into PL group and distant group according to their paired metastatic sites (Figure 5D). All patients in the PL group were stage M1a, that is, cancer was confined to the thoracic cavity[28]. Results showed the CD8+ T cell level in the primary tumors with PL metastases and distant metastases were not significantly different (Figure 5E) which was probably due to the small sample size; however, the CD4+ T cell level in the primary tumors with distant metastases was significantly higher than that in the primary tumors with PL metastases ($P = 0.00048$, Figure 5F), and TPS level also showed a similar trend as CD4 ($P = 0.059$, Figure 5G). Same results were obtained using dichotomized CD8, CD4 and TPS status (Supplementary Fig.S5A-S5C).

A key role of Th2/Th1 CD4+ T cell subsets in determining metastatic potential: validation by TCGA data and a single cell RNA-sequencing dataset

As described in the "Method" section, we downloaded the enrichment score data of 64 immune and stromal cell types in the TCGA lung adenocarcinoma primary tumors, which were pre-calculated by xCell[14], and divided 402 primary
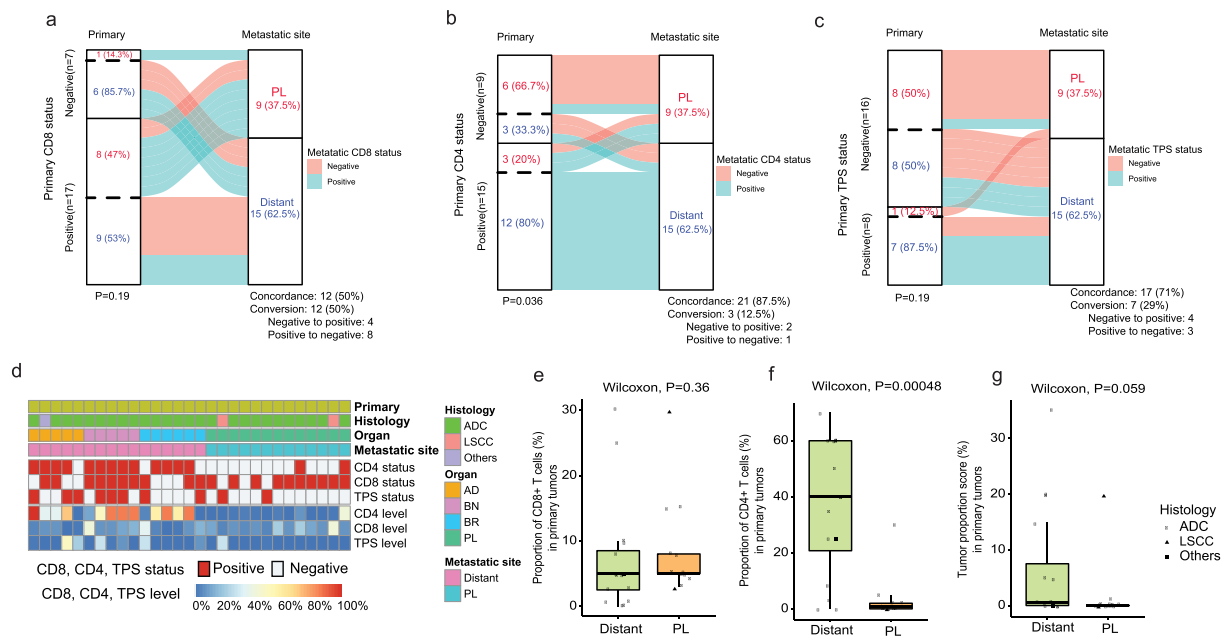
Figure 5. Association of immune status of primary tumors and metastatic sites. (A)-(C) change of CD8 status (A), CD4 status (B) and TPS status (C) from primary tumors to paired PL and distant metastases (n = 24 pairs). The color of bands represents status of CD8, CD4 or TPS in the metastases. For example, in (A), a cyan-color band starting from CD8-negative primary tumors (the left) to PL metastases (the right) stands for CD8 status changed from negative in the primary tumors to positive in the PL metastases. The width of the bands represents the proportion of corresponding cases. Concordance represents the status of CD8, CD4 or TPS did not change from primary tumors to metastases. The dashed lines in the left bar divide the metastatic destinations into PL and distant metastases (BR/BN/AD). P value was calculated by Fisher exact test. (D) distribution of the levels of CD8+ T cells, CD4+ T cells and TPS as well as CD8, CD4 and TPS status in the primary tumors (n = 29) with different metastatic organs. Five primary tumors having PL metastases and one primary tumor having bone metastasis were also included to increase sample number, although they lacked genomic and immune information of paired metastases. One patient with both PL and bone metastasis was included into the distant group. (E)-(G) comparison of CD8+ T cells (E), CD4+ T cells (F) and TPS (G) level in the primary tumors with PL metastasis (n = 13) or distant metastasis (BR/BN/AD, n = 16). One patient had both PL metastasis and bone metastasis. This patient was classified into distant group. PL: pleural; BR: brain; BN: bone; AD: adrenal gland; TPS: tumor proportion score.

tumors into 4 groups based on metastatic situation. Unfortunately, there were only two cases with M1a stage, i.e., intrathoracic metastasis such as PL metastasis; we could not directly compare PL metastasis with distant metastasis as we did in our cohort. However, we were still able to investigate the association of the immune background of primary tumors with metastatic sites based on the stepwise metastasis of lymph node and distant metastasis. Differential analysis showed that Th1 and Th2, two subsets of CD4+ T cells, were significantly enriched in the metastatic group (M, N2-N3, and N1) compared with N0-M0 group (q = 0.03, $\log_2$FC = 0.20 for Th1; q = 0.04, $\log_2$FC = 0.39 for Th2); on the contrary, CD8+ T cells were significantly enriched in the non-metastatic group (N0-M0) (q = 0.016, $\log_2$FC=−0.54) (Supplementary Fig.S6). The enrichment of majorities of CD8 T+ cell subsets (Supplementary Fig.S7A) and CD4 T+ cell subsets except Th1 and Th2 (Supplementary Fig.S7B) showed a decreasing trend from N0-M0 to M group. In contrast, two CD4+ T cell subsets, Th1 and Th2, showed an increasing trend, which was consistent with our previous finding that primary tumors with local metastases (PL) had a higher CD4+ T cell level than those with distant metastases. Additionally, although both Th1 and Th2 had the same change direction, their change rate may be different. As a result, the ratio of Th2 to Th1 increased significantly from N0-M0 to M group (Supplementary Fig.S7C), suggesting a Th1 to Th2 shift may be associated with metastatic potential of lung adenocarcinoma. Other tumor infiltration immune cells (TIICs), such as B cells (Supplementary Fig. S7D) and DC cells (Supplementary Fig.S7E) also showed a decreasing trend from N0-M0 group to M group; macrophage cells were not significantly changed (Supplementary Fig. S7F); whereas epithelial cells, representing tumor cells, showed an increasing trend (Supplementary Fig.S7G). In single-cell analysis, although due to lack of Th2 annotation in the reference atlas, the change of the proportion of Th2 subset could not be tracked, we could still see the proportion of Th1 cells accounting for lung cancer tissue T cell population increased from stage I to stage IV (Supplementary Fig.S8A-S8B). On the contrary, the proportion of CD8+ T cell subsets decreased, particularly in stage IV, which further supported our previous results.

Immune landscape of primary and its dynamic change toward metastasis affects survival

We next assessed whether immune status of primary tumors would affect patient's progression. We only included primary tumors with synchronous metastases (n = 22) (Supplementary Fig.S1), which had a unique PFS definition. Patients with CD8-positive primary tumor exhibited a better PFS than those with CD8-negative primary tumor (P = 0.099) (Supplementary Fig. S9A). Among 22 cases, 5 cases had CD8 positive-to-negative conversion. Despite CD8-positive cases in general having a better PFS than CD8-negative cases, the 5 cases with positive-to-negative conversion tended to have a worse PFS and no better than CD8-negative cases (P = 0.70) (Supplementary Fig.S9B). On the contrary, patients with CD4-negative primary tumors were associated with a better PFS (P = 0.044) (Supplementary Fig.S9C). When combining CD8 and CD4

status, we found that CD8-positive/CD4-negative cases had the best PFS (Supplementary Fig.S9D). TPS status was not associated with PFS significantly (Supplementary Fig.S9E). As expected, polyploid primary tumors, which tended to have a lower CD8+ T cell (Figure 3A) was associated with a worse PFS (p = 0.049) (Supplementary Fig.S9F). In fact, multivariate Cox analysis on the basis of the TCGA data set also showed the enrichment of Th2 subset and CD8+ T cell in primary tumor was associated with patient's prognosis. The high enrichment of Th2 in primary tumor predicted a worse overall survival; while the high enrichment of CD8+ T cell predicted a better overall survival after being adjusted by age, sex, and pathological stage (Supplementary Fig.S10).

Discussion

In this study, we investigated possible immune evolutionary pathways for local (pleural) and distant metastases. Our findings aligned with earlier research, showing that distant metastases exhibit greater chromosomal instability (CIN)[29,30] and immunosuppression as indicated by reduced infiltration of CD8+ T cells[6,7] compared with the primary tumors. Additionally, we identified a negative association between CIN and CD8+ T cell level, which has also been reported in previous studies[9,31]. Our study revealed that acquired DDR deficiency is probably a key factor to drive the immunosuppression conversion in the distant metastases. One possible explanation is that acquired DDR deficiency exacerbated CIN, which in turn triggers immunosuppression through the cGAS-STING pathway[10–12–32]. While our study did not delve into the precise molecular mechanisms of this pathway, it did provide compelling clinical evidence that acquired DDR plays a crucial role in the immune evolution of distant metastases. As such, targeting DDR machinery may be a promising strategy for inhibiting metastasis.

In contrast to distant metastases, local metastases exhibit genomic and immune profiles that are similar to those of the primary tumors. Therefore, we propose that local metastases follow a different immune evolutionary pathway, whereby they inherit the immune and genomic characteristics of the primary tumors. A noteworthy discovery is that local metastases had significantly lower level of CD4+ T cells compared to distant metastases. This cannot be explained by the dynamic change of CD4+ T cells in the metastases (such as decreasing in local metastases or increasing in distant metastases) since the CD4+ T cell status generally remained constant between the metastases and primary tumors. Our research indicated that primary tumors with elevated CD4+ T cell levels were more likely to metastasize distantly rather than locally. We postulate that the immune competence of the primary tumors may hinder distant metastasis, while immunosuppressed primary tumors may have a greater potential to spread to distant organs. For example, pleural metastasis via visceral pleural invasion[33] may require less demanding for immune conditions compared with distant metastasis.

Using both the TCGA dataset and a single-cell RNA-seq dataset, we discovered that CD4+ T helper cells, specifically Th1 and Th2 cells, may play a pivotal role in determining the metastatic potential of primary tumors. The TCGA data revealed an

increasing trend in the abundance of Th1 and Th2 cells with increasing metastatic distance (from proximal lymph nodes to distal lymph nodes to distant organs) Additionally, the ratio of Th2 to Th1 also significantly increased with metastatic distance. A recent study[34] showed Th2 subset, which has a potential to promote tumor growth by secreting immunosuppressive cytokines[35], was dominated in both lung cancer tissue and peritumoral lymph nodes. Previous studies also observed Th2 skewing in bladder cancer[36], kidney cancer[37], breast, and lung cancer[38]. An animal study has found that Th2 cells promote lung metastasis of breast cancer in a CD8-independent way[39,40]. Based on the evidence, we suppose that Th1 and Th2, particularly Th2 in primary tumors may determine their metastatic potential, which needs further study to verify since other CD4+ T cell subsets, such as Th9, Th17 and Treg are also found to promote metastasis[41,42].

In a similar manner to CD4+ T cells, tumors with high levels of PD-L1 were found to be linked to distant metastases. Experiments have shown that PD-L1 promotes the migration and invasion of gastric cancer cells[43,44], and lung cancer cells[45], and its upregulation occurs early on in precancerous tissues of lung squamous cell carcinoma[46]. Numerous studies have demonstrated that PD-L1 is significantly associated with advanced tumor stages, as well as lymph node and distant metastases in various types of cancers[47] including NSCLC[48].

Based on these findings, we propose two types of immune evolutionary modes for distant and local metastases (Supplementary Fig.S11). Some primary tumors exhibit immunosuppression, which is distinguished by low levels of TIICs (such as CD8+ T cells), elevated levels of CD4+ T cells (specifically Th1 and Th2 subsets) and high PD-L1. On the other hand, there may be primary tumors with immunocompetence, which is identified by high levels of TIICs, low CD4+ T cells, and low PD-L1. Tumors with immunosuppression have the potential to overcome the immune barrier and metastasize to distant organs. During metastasis, immunosuppression may develop which is driven by acquired DDR deficiency. Conversely, tumors with immunocompetence tend to metastasize locally and typically maintain the immune and genomic profiles of the primary tumor. In conclusion, our study demonstrates a potential mechanism that distant metastases acquire immunosuppression through DDR deficiency and reveal the important role of certain CD4 T cell subpopulations such as Th2 and Th1 in the process of metastasis, so that providing new targets for assessment of metastatic potential of primary tumors as well as intervention of metastasis in lung cancer.

Disclosure statement

No potential conflict of interest was reported by the authors.

Funding

ORCID

Wen-Fang Tang http://orcid.org/0000-0001-6116-6838

Author contributions

Wen-Fang Tang, Xiao-Jun Fan, Hua Bao, Yi Liang, Rui Fu, Yi-Long Wu and Wen-Zhao Zhong contributed to conception, design of the study, formal analysis and manuscript writing. Wen-Fang Tang and Xiao-Jun Fan contributed to statistical analysis, visualization and manuscript writing. Wen-Fang Tang, Yi Liang, Min Wu, Chao Zhang and Jian Su designed, supervised and provided resources for this study. All authors contributed to manuscript revision, read, and approved the submitted version.

Availability of data and materials

Most data were shown in Supplementary Tables , and other data if need could contact syzhongwenzhao@scut.edu.cn or WenfangTang2022@outlook.com.

Consent for publication

All authors have approved the publication.

Ethics approval and consent to participate

This study was approved by the ethics and scientific committees of Guangdong Provincial People's Hospital (no. KY-Q-2022-391-01).

References

1. Gandhi L, Rodríguez-Abreu D, Gadgeel S, Esteban E, Felip E, De Angelis F, Domine M, Clingan P, Hochmair MJ, Powell SF, et al. Pembrolizumab plus chemotherapy in metastatic non-small-cell lung cancer. N Engl J Med. 2018;378 (22):2078–2092.

2. Ramalingam SS, Vansteenkiste J, Planchard D, Cho BC, Gray JE, Ohe Y, Zhou C, Reungwetwattana T, Cheng Y, Chewaskulyong B, et al. Overall survival with osimertinib in untreated, EGFR-mutated advanced NSCLC. N Engl J Med. 2020;382 (1):41–50.

3. Dillekås H, Rogers MS, Straume O. Are 90% of deaths from cancer caused by metastases? Cancer Med. 2019;8(12):5574–5576. doi:10. 1002/cam4.2474.

4. Kitamura T, Qian BZ, Pollard JW. Immune cell promotion of metastasis. Nat Rev Immunol. 2015;15:73–86.

5. Müller P, Rothschild SI, Arnold W, Hirschmann P, Horvath L, Bubendorf L, Savic S, Zippelius A. Metastatic spread in patients with non-small cell lung cancer is associated with a reduced density of tumor-infiltrating T cells. Cancer Immunol Immunother. 2016;65:1–11.

6. Lee WC, Reuben A, Hu X, McGranahan N, Chen R, Jalali A, Negrao MV, Hubert SM, Tang C, Wu CC, et al. Multiomics profiling of primary lung cancers and distant metastases reveals immunosuppression as a common characteristic of tumor cells with metastatic plasticity. Genome Biol. 2020;21 (1):271.

7. Kudo Y, Haymaker C, Zhang J, Reuben A, Duose DY, Fujimoto J, Roy-Chowdhuri S, Solis Soto LM, Dejima H, Parra ER, et al. Suppressed immune microenvironment and repertoire in brain metastases from patients with resected non-small-cell lung cancer. Ann Oncol. 2019;30(9):1521–1530.

8. Nguyen DX, Massagué J. Genetic determinants of cancer metastasis. Nat Rev Genet. 2007;8:341–352.

9. Davoli T, Uno H, Wooten EC, Elledge SJ. Tumor aneuploidy correlates with markers of immune evasion and with reduced response to immunotherapy. Sci. 2017;355(6322). doi:10.1126/science.aaf8399.

10. Bakhoum SF, Ngo B, Laughney AM, Cavallo JA, Murphy CJ, Ly P, Shah P, Sriram RK, Watkins TBK, Taunk NK, et al. Chromosomal instability drives metastasis through a cytosolic DNA response. Nature. 2018;553(7689):467–472.

11. Motwani M, Pesiridis S, Fitzgerald KA. DNA sensing by the Cgas-STING pathway in health and disease. Nat Rev Genet. 2019;20:657–674.

12. Xu Y, Nowsheen S, Deng M. DNA repair deficiency regulates immunity response in cancers: molecular mechanism and approaches for combining immunotherapy. Cancers (Basel). 2023;15:1619.

13. Klapp V, Alvarez-Abril B, Leuzzi G, Kroemer G, Ciccia A, Galluzzi L. The DNA damage response and inflammation in cancer. Cancer Discov. 2023;OF1–25.

14. Aran D, Hu Z, Butte AJ. xCell: digitally portraying the tissue cellular heterogeneity landscape. Genome Biol. 2017;18:220.

15. Guo X, Zhang Y, Zheng L, Zheng C, Song J, Zhang Q, Kang B, Liu Z, Jin L, Xing R, et al. Global characterization of T cells in non-small-cell lung cancer by single-cell sequencing. Nat Med. 2018;24(7):978–985.

16. Hao Y, Hao S, Andersen-Nissen E, Mauck WM, Zheng S, Butler A, Lee MJ, Wilk AJ, Darby C, Zager M, et al. Integrated analysis of multimodal single-cell data. Cell. 2021;184(13):3573–87 e29.

17. Andreatta M, Corria-Osorio J, Muller S, Cubas R, Coukos G, Carmona SJ. Interpretation of T cell states from single-cell transcriptomics data using reference atlases. Nat Commun. 2021;12:2965.

18. Bolger AM, Lohse M, Usadel B. Trimmomatic: a flexible trimmer for illumina sequence data. Bioinformatics. 2014;30(15):2114–2120. doi:10.1093/bioinformatics/btu170.

19. Li H, Durbin R. Fast and accurate long-read alignment with burrows-wheeler transform. Bioinformat. 2010;26:589–595.

20. McKenna A, Hanna M, Banks E, Sivachenko A, Cibulskis K, Kernytsky A, Garimella K, Altshuler D, Gabriel S, Daly M, et al. The genome analysis toolkit: a mapreduce framework for analyzing next-generation DNA sequencing data. Genome Res. 2010;20(9):1297–1303.

21. Cibulskis K, Lawrence MS, Carter SL, Sivachenko A, Jaffe D, Sougnez C, Gabriel S, Meyerson M, Lander ES, Getz G. Sensitive detection of somatic point mutations in impure and heterogeneous cancer samples. Nat Biotechnol. 2013;31:213–219.

22. Shen R, Seshan VE. FACETS: allele-specific copy number and clonal heterogeneity analysis tool for high-throughput DNA sequencing. Nucleic Acids Res. 2016;44:e131.

23. Franch-Expósito S, Bassaganyas L, Vila-Casadesús M, Hernández-Illán E, Esteban-Fabró R, Díaz-Gay M, Lozano JJ, Castells A, Llovet JM, Castellví-Bel S, et al. Cnapp, a tool for the quantification of copy number alterations and integrative analysis revealing clinical implications. Elife. 2020;9.

24. Alexandrov LB, Kim J, Haradhvala NJ, Huang MN, Tian Ng AW, Wu Y, Boot A, Covington KR, Gordenin DA, Bergstrom EN, et al. The repertoire of mutational signatures in human cancer. Nature. 2020;578(7793):94–101.

25. Martincorena I, Raine KM, Gerstung M, Dawson KJ, Haase K, Van Loo P, Davies H, Stratton MR, Campbell PJ. Universal patterns of selection in cancer and somatic tissues. Cell. 2018;173:1823.

26. Roth A, Khattra J, Yap D, Wan A, Laks E, Biele J, Ha G, Aparicio S, Bouchard-Côté A, Shah SP. PyClone: statistical inference of clonal population structure in cancer. Nat Methods. 2014;11:396–398.

27. Juneja VR, McGuire KA, Manguso RT, LaFleur MW, Collins N, Haining WN, Freeman GJ, Sharpe AH. PD-L1 on tumor cells is sufficient for immune evasion in immunogenic tumors and inhibits CD8 T cell cytotoxicity. J Exp Med. 2017;214:895–904.

28. Detterbeck FC, Boffa DJ, Kim AW, Tanoue LT. The eighth edition lung cancer stage classification. Chest. 2017;151(1):193–203. doi:10.1016/j.chest.2016.10.010.

29. Thorsson V, Gibbs DL, Brown SD, Wolf D, Bortone DS, Ou Yang TH, Porta-Pardo E, Gao GF, Plaisier CL, Eddy JA, et al. The immune landscape of cancer. Immunity. 2018;48(4):812–30. e14.

30. Birkbak NJ, McGranahan N. Cancer genome evolutionary trajectories in metastasis. Cancer Cell. 2020;37(1):8–19. doi:10.1016/j.ccell.2019.12.004.

31. Bassaganyas L, Pinyol R, Esteban-Fabró R, Torrens L, Torrecilla S, Willoughby CE, Franch-Expósito S, Vila-Casadesús M, Salaverria I, Montal R, et al. Copy-number alteration burden differentially impacts immune profiles and molecular features of hepatocellular carcinoma. Clin Cancer Res. 2020;26(23):6350–6361.

32. Galluzzi L, Vanpouille-Box C, Bakhoum SF, Demaria S. SnapShot: cGAS-STING signaling. Cell. 2018;173(1):276- e1. doi:10.1016/j.cell.2018.03.015.

33. Agalioti T, Giannou AD, Stathopoulos GT. Pleural involvement in lung cancer. J Thorac Dis. 2015;7:1021–1030.

34. Frafjord A, Buer L, Hammarström C, Aamodt H, Woldbæk PR, Brustugun OT, Helland Å, Øynebråten I, Corthay A. The immune landscape of human primary lung tumors is Th2 skewed. Front Immunol. 2021;12:764596.

35. Disis ML. Immune regulation of cancer. J Clin Oncol. 2010;28:4531–4538.

36. Satyam A, Singh P, Badjatia N, Seth A, Sharma A. A disproportion of TH1/TH2 cytokines with predominance of TH2, in urothelial carcinoma of bladder. Urol Oncol. 2011;29:58–65.

37. Li L, Yang C, Zhao Z, Xu B, Zheng M, Zhang C, Min Z, Guo J, Rong R. Skewed T-helper (Th)1/2- and Th17/T regulatory-cell balances in patients with renal cell carcinoma. Mol Med Rep. 2015;11:947–953.

38. Caras I, Grigorescu A, Stavaru C, Radu DL, Mogos I, Szegli G, Salageanu A. Evidence for immune defects in breast and lung cancer patients. Cancer Immunol Immunother. 2004;53:1146–1152.

39. DeNardo DG, Barreto JB, Andreu P, Vasquez L, Tawfik D, Kolhatkar N, Coussens LM. CD4(+) T cells regulate pulmonary metastasis of mammary carcinomas by enhancing protumor properties of macrophages. Cancer Cell. 2009;16:91–102.

40. Pardoll D. Metastasis-promoting immunity: when T cells turn to the dark side. Cancer Cell. 2009;16(2):81–82. doi:10.1016/j.ccr.2009.07.007.

41. Yang P, Li QJ, Feng Y, Zhang Y, Markowitz G, Ning S, Deng Y, Zhao J, Jiang S, Yuan Y, et al. TGF-β-miR-34a-CCL22 signaling-induced treg cell recruitment promotes venous metastases of HBV-positive hepatocellular carcinoma. Cancer Cell. 2012;22(3):291–303.

42. Salazar Y, Zheng X, Brunn D, Raifer H, Picard F, Zhang Y, Winter H, Guenther S, Weigert A, Weigmann B, et al. Microenvironmental Th9 and Th17 lymphocytes induce

metastatic spreading in lung cancer. J Clin Invest. 2020;130 (7):3560–3575.

43. Li Y, Yang X, Wu Y, Zhao K, Ye Z, Zhu J, Xu X, Zhao X, Xing C. B7-H3 promotes gastric cancer cell migration and invasion. Oncotarget. 2017;8:71725–71735.

44. Dai W, Shen G, Qiu J, Zhao X, Gao Q. Aberrant expression of B7-H3 in gastric adenocarcinoma promotes cancer cell metastasis. Oncol Rep. 2014;32:2086–2092.

45. Yu W, Hua Y, Qiu H, Hao J, Zou K, Li Z, Hu S, Guo P, Chen M, Sui S, et al. PD-L1 promotes tumor growth and progression by activating WIP and β-catenin signaling pathways and predicts poor prognosis in lung cancer. Cell Death & Disease. 2020;11(7):506.

46. Angelova M, Mascaux C, Galon J. Evasion before invasion: pre-cancer immunosurveillance. Oncoimmunology. 2021;10 (1):1912250. doi:10.1080/2162402X.2021.1912250.

47. Yu J, Wang X, Teng F, Kong L, Yu J. PD-L1 expression in human cancers and its association with clinical outcomes. Onco Targets Ther. 2016;9:5023–5039.

48. Chen YB, Mu CY, Huang JA. Clinical significance of programmed death-1 ligand-1 expression in patients with non-small cell lung cancer: a 5-year-follow-up study. Tumori. 2012;98:751–755.